

# Universal transition of spectral fluctuation in particle-hole symmetric system

Triparna Mondal<sup>1\*</sup> and Shashi C. L. Srivastava<sup>1,2</sup>

<sup>1\*</sup>Variable Energy Cyclotron Centre, Kolkata 700064, India..

<sup>2</sup>Homi Bhabha National Institute, Training School Complex, Anushaktinagar, Mumbai - 400094, India.

\*Corresponding author(s). E-mail(s): [t.mondal@vecc.gov.in](mailto:t.mondal@vecc.gov.in);

## Abstract

We study the spectral properties of a multiparametric system having particle-hole symmetry in random matrix setting. We observe a crossover from Poisson to Wigner-Dyson like behavior in average local ratio of spacing within a spectrum of single matrix as a function of effective single parameter referred to as complexity parameter. The average local ratio of spacing varies logarithmically in complexity parameter across the transition. This behavior is universal for different ensembles subjected to same matrix constraint like particle-hole symmetry. The universality of this dependence is further established by studying interpolating ensemble connecting systems with particle-hole symmetry to that with chiral symmetry. For each interpolating ensemble the behavior remains logarithmic in complexity parameter. We verify this universality of spectral fluctuation in case of a 2D Su-Schrieffer-Heeger (SSH) like model along with the logarithmic dependence on complexity parameter for ratio of spacing during transition from integrable to non-integrable limit.

**Keywords:** random matrices, level statistics, particle-hole symmetry, 2D SSH model

## 1 Introduction

Statistical behavior of a complex system modeled by a random matrix ensemble (RME) requires information of different constraints imposed on the Hamiltonian matrix representing the system [1–4]. The constraints influencing the nature of a system-dependent RME are categorized in two broad types: a) *matrix or global constraints* which mainly

affect broad structure of single matrix governing the system; b) *ensemble or local constraints* which specify the distribution properties of the matrix elements [1, 2]. The symmetries are one of the examples of matrix constraints whereas disorder in the matrix elements is an example of ensemble constraints [1–3]. Matrix constraints time-reversal symmetry and spin-rotation symmetry together lead the RME to Gaussian orthogonal ensemble (GOE) as it becomes invariant under orthogonal transformation [1, 2]. Absence of both or one of these symmetries leads to the other two ensembles (Gaussian unitary ensemble (GUE) and Gaussian symplectic ensemble (GSE), respectively) of Dyson’s three-fold way of canonical transformations. Beyond this classification, three chiral symmetric and four particle-hole symmetric ensembles were introduced later along with or without time-reversal and spin-rotation symmetry [5]. The choice of independence of matrix elements leads to Gaussianity of the distribution, and further specification of ensemble constraints like mean and variance of the disorder distribution of the matrix elements lead to different kind of ensembles. Alternatively, one could add the correlation in the matrix elements to achieve the same [3, 6–9]. Variation of ensemble parameters alone has been shown to drive the system from Poissonian limit to Wigner-Dyson statistics (*e.g.* metal-insulator transition in Anderson ensemble [10]). Moreover, irrespective of ensemble parameters, the local spectral statistics for different ensembles belonging to same matrix constraint group show similar behavior based on the *ensemble complexity parameter* [6–9, 11, 12]. This is a single parameter representing the degree and nature of complexity in the system defined as a scaled logarithmic function of all parameters of the ensemble. This complexity parameter based universality of spectral fluctuations for different ensembles with and without chiral symmetry for Dyson’s Gaussian ensembles were studied in [6] and [7, 8, 11] respectively based on the complexity parameter. It is natural to ask if this type of universality remains preserved for different ensembles with matrix constraint particle-hole symmetry, completing the additional symmetry classes considered in [5]. This symmetry naturally occurs in various physical systems, one of the well known cases is Andreev reflection at the interface of the normal metal-superconducting systems leaving the associated Hamiltonian invariant under this symmetry [13]. The standard Hamiltonian used for these systems is the Bardeen-Cooper-Schrieffer (BCS) Hamiltonian which can be expressed in terms of another Hermitian operator, known as Bogoliubov deGennes (BdG) Hamiltonian (Eq. 1) [13–16]. The Su-Schrieffer-Heeger (SSH) model is a topological example of particle-hole symmetric Hamiltonian. The one dimensional representation of this model is popular to investigate topological phenomena in condensed matter physics [17–19]. Later, people generalized this model to several types of two dimensional (2D) SSH model to study different properties of topology [20–30]. For further appearances of particle-hole symmetry in condensed matter physics, see reference [17]. Considering the Hamiltonian matrix with particle-hole symmetry described in the site basis, the off-diagonal blocks of it represent the hopping of the particles (electrons or holes) from one site to others while the onsite dynamics of those particles are represented by its diagonal blocks [1, 5, 31–33]. The latter ones are considered to be zero if the system has chiral symmetry instead of particle-hole symmetry [1, 32–34]. A transition from particle-hole to chiral symmetry can be achieved by controlling the ensemble parameters of the diagonal blocks of Hamiltonian matrix.

Motivated by this, we ask two specific but related questions: a) Whether transition from Poissonian to Wigner-Dyson like behavior within single spectrum is governed by the complexity parameter and show universality for different ensembles respecting the particle-hole symmetry as matrix constraint? and b) Whether each point of transition from particle-hole to chiral symmetric ensembles respects this universality?

In this paper we consider time-reversal symmetric systems with integer spin having particle-hole symmetry. In section 2, we introduce the matrix representation of the Hamiltonian and discuss the relevant symmetries along with the ensemble density. We formulate single parametric representation of multiparametric evolution of matrix elements in section 3 following the steps for other symmetry classes discussed in [6–9]. Section 4 details three different ensembles arising due to different ensemble constraint even though they satisfy the same matrix constraint. In section 5, we present our studies on spectral statistics across the spectrum and show that Poisson to Wigner-Dyson transition is independent of the ensembles considered. We propose an interpolating ensemble from particle-hole to chiral symmetry in section 6 and study the ratio of nearest neighbor spacing distribution. We show that at each interpolating point, the transition across the spectrum remains identical for different ensembles. These findings are further corroborated by studying a dynamical model of 2D SSH type in section 7. The summary and outlook follows in section 8.

## 2 Multiparametric Gaussian ensemble with particle-hole symmetry and other matrix constraints

A  $2N \times 2N$  Hamiltonian matrix with particle-hole symmetry (also known as BdG Hamiltonian) can be described as

$$H_{ph} = \begin{pmatrix} \mathcal{H} & \Delta \\ \Delta^\dagger & -\mathcal{H}^T \end{pmatrix} \quad (1)$$

with  $\mathcal{H}$  is a  $N \times N$  hermitian block matrix:  $\mathcal{H} = \mathcal{H}^\dagger$  and  $\Delta$  is a  $N \times N$  anti-symmetric block matrix, *i.e.*  $\Delta = -\Delta^T$  due to Fermi statistics [1, 2, 5].

The particle-hole symmetry exchanges electrons with holes. Considering an antiunitary operator  $\mathcal{P} = \sigma_x \mathcal{K}$ , where  $\mathcal{K}$  is the complex conjugation operator and  $\sigma_x$  is the Pauli matrix acting on the blocks. Therefore, the Hamiltonian in Eq. 1 can be described as

$$H_{ph} = -\mathcal{P}H_{ph}\mathcal{P}^{-1}. \quad (2)$$

The minus sign due to the particle-hole symmetry implies the spectrum of  $H_{ph}$  must be symmetric around zero energy and for every eigenvector  $\psi$  of  $H_{ph}$  with energy  $E$ , there will be a particle-hole symmetric eigenvector  $\mathcal{P}\psi$  with energy  $-E$ .

If time-reversal symmetry along with spin-rotation symmetry is also present in the system with particle-hole symmetry, the Hamiltonian  $H_{ph}$  become invariant under orthogonal transformation and hence, the matrix elements become real. Now both the

blocks  $\mathcal{H}$  and  $\Delta$  become real

$$\mathcal{H} = \mathcal{H}^* = \mathcal{H}^T \quad (3)$$

$$\Delta = \Delta^T. \quad (4)$$

Therefore, the Hamiltonian  $H_{ph}$  in Eq. 1 will look like

$$H = \begin{pmatrix} \mathcal{H} & \Delta \\ \Delta & -\mathcal{H} \end{pmatrix}. \quad (5)$$

This is called class CI of particle-hole symmetry. In this paper, we confine our study only to this CI class. The number of independent elements in  $H$  now reduced to  $N(N+1)$  from  $4N^2$ . The results we have achieved in this paper are intuitively true for the other three classes of particle-hole symmetry in qualitative manner; although the technical difficulties in the calculation would increase.

The joint probability distribution function of the ensemble of such matrices is given by

$$\rho(H) = \rho_{\mathcal{H}}(\{H_{k,l}\})\rho_{\Delta}(\{H_{k,l+N}\}) \quad (6)$$

with  $k, l$  going from  $1 \rightarrow N$ . The additional constraints of sum of diagonal blocks and difference of off-diagonal blocks giving null matrices have been taken into account to write Eq. 5.  $\rho_{\mathcal{H}}(\mathcal{H})$  and  $\rho_{\Delta}(\Delta)$  in Eq. 6 are the probability densities of the ensemble of real symmetric  $\mathcal{H}$  and  $\Delta$  matrices respectively, defined as

$$\rho_{\mathcal{H}}(\mathcal{H}, h, b) = \mathcal{C}_{\mathcal{H}} \exp \left[ - \sum_{k \leq l=1}^N \frac{1}{2h_{kl}^{(\mathcal{H})}} (\mathcal{H}_{kl} - b_{kl}^{(\mathcal{H})})^2 \right] \quad (7)$$

$$\rho_{\Delta}(\Delta, h, b) = \mathcal{C}_{\Delta} \exp \left[ - \sum_{k \leq l=1}^N \frac{1}{2h_{kl}^{(\Delta)}} (\Delta_{kl} - b_{kl}^{(\Delta)})^2 \right] \quad (8)$$

where  $\mathcal{C}_{\mathcal{H}}$  and  $\mathcal{C}_{\Delta}$  are normalization constants. All the matrix elements are independent and identically distributed and taken randomly from a Gaussian distribution with variances  $h_{kl}^{(\mathcal{H})}$  and  $h_{kl}^{(\Delta)}$  and means  $b_{kl}^{(\mathcal{H})}$  and  $b_{kl}^{(\Delta)}$ . Using  $H_{kl} = \mathcal{H}_{kl}$  and  $H_{k,N+l} = \Delta_{kl}$ , the ensemble density of  $H$  becomes

$$\rho(H, h, b) = \mathcal{C} \exp \left[ - \sum_{k \leq l=1}^N \frac{1}{2h_{kl}} (H_{kl} - b_{kl})^2 - \sum_{k \leq l=1}^N \frac{1}{2h_{k,N+l}} (H_{k,N+l} - b_{k,N+l})^2 \right], \quad (9)$$

Let us define  $h \equiv [h_{kl}]$  and  $b \equiv [b_{kl}]$  to be the matrices for variances and means respectively. Clearly, with different choices of ensemble constraints *i.e.*  $h$  and  $b$ , it is possible to achieve different ensembles with particle-hole symmetry. We discuss three of them later in this paper.

### 3 Diffusion of matrix elements: Ensemble complexity parameter

Considering our system (Eq. 5) evolves in the block matrix space by a continuous variation of multiple parameters ( $h_{kl}$  and  $b_{kl}$  in our case), preserving the global symmetries in a suitable basis, we can use previously studied idea of the diffusion of the density depending on the multiple parameters via a single averaged logarithmic function  $Y$  referred to as the ensemble complexity parameter [6–9]. The diffusion equation connects evolution in parametric space to that in matrix space.  $\mathcal{H}$  and  $\Delta$  themselves being Hermitian, following [7], single parametric diffusion equation of  $\rho_{\mathcal{H}}(\mathcal{H})$  and  $\rho_{\Delta}(\Delta)$  in matrix space is given by,

$$\frac{\partial \rho_{\mathcal{H}}}{\partial Y_{\mathcal{H}}} = \sum_{k,l} \frac{\partial}{\partial \mathcal{H}_{kl}} \left[ \left( \frac{1 + \delta_{kl}}{2} \right) \frac{\partial \rho_{\mathcal{H}}}{\partial \mathcal{H}_{kl}} + \gamma \mathcal{H}_{kl} \rho_{\mathcal{H}} \right] \quad (10)$$

$$\frac{\partial \rho_{\Delta}}{\partial Y_{\Delta}} = \sum_{k,l} \frac{\partial}{\partial \Delta_{kl}} \left[ \left( \frac{1 + \delta_{kl}}{2} \right) \frac{\partial \rho_{\Delta}}{\partial \Delta_{kl}} + \gamma \Delta_{kl} \rho_{\Delta} \right] \quad (11)$$

where the complexity parameters  $Y_{\mathcal{H}}$  and  $Y_{\Delta}$  are,

$$Y_{\mathcal{H}} = -\frac{1}{2M_{\mathcal{H}}\gamma} \ln \left[ \prod_{k \leq l=1}^N |1 - \gamma g_{kl} h_{kl}^{(\mathcal{H})}| |b_{kl}^{(\mathcal{H})}|^2 \right] + C_{\mathcal{H}} \quad (12)$$

$$Y_{\Delta} = -\frac{1}{2M_{\Delta}\gamma} \ln \left[ \prod_{k \leq l=1}^N |1 - \gamma g_{kl} h_{kl}^{(\Delta)}| |b_{kl}^{(\Delta)}|^2 \right] + C_{\Delta} \quad (13)$$

with  $g_{kl} = 2 - \delta_{kl}$  while  $\gamma$  is taken as arbitrary parameter. Here  $M_{\mathcal{H}} = M_{\Delta} \equiv M$  (since size, symmetry and matrix elements distribution of  $\mathcal{H}$  and  $\Delta$  are same.) is the number of non-zero  $h_{kl}$  and  $b_{kl}$  and the  $\prod$ s are over them.  $C_{\mathcal{H}}$  and  $C_{\Delta}$  are the integration constants. Therefore, the solution of complexity parameter for  $\rho(H)$  (Eq. 9) is

$$Y = -\frac{1}{2M\gamma} \left[ \ln \left\{ \prod_{k \leq l=1}^N |1 - \gamma g_{kl} h_{kl}| |b_{kl}|^2 \right\} + \ln \left\{ \prod_{k \leq l=1}^N |1 - \gamma g_{kl} h_{k,N+l}| |b_{k,N+l}|^2 \right\} \right] + \text{const.} \quad (14)$$

It is expected that diffusion of density would lead to an evolution in the spectral properties of the systems. We next explore this numerically for the system with particle-hole symmetry. The spectral fluctuation is dependent on the ensemble constraints and due to non-stationarity of the spectrum, it is necessary to rescale the complexity parameter  $Y$  by the square of local mean level spacing  $\Delta_l(e)$  at the spectral

point of interest (say  $e$ ). The re-scaled complexity parameter  $\Lambda$  can be written as

$$\Lambda(e, Y) = \frac{Y - Y_0}{\Delta_l^2(e)} \quad (15)$$

with  $Y_0$  being the complexity parameter of initial state at the start of evolution. Since the eigenstates are not always expected to be exactly delocalized,  $\Delta_l(e)$  strongly depends on energy range. It corresponds to states which are interacting at energy  $e$  only. As we know, localized eigenstates in different parts of the basis space do not interact, we expect  $\Delta_l(e)$  is proportional to average correlation at energy  $e$ . Therefore, an acceptable definition of this can be

$$\Delta_l(e) \equiv \frac{1}{\langle \rho_{loc}(e) \rangle}, \quad \text{with } \rho_{loc}(e) \equiv \sum_n \phi_n \delta(e - e_n) \quad (16)$$

where  $\phi_n$  is the  $n^{\text{th}}$  eigenfunction overlapping with other eigenfunctions in the energy range  $e$  and  $e \pm \delta e$  [6]. The sum in Eq. 16 is over only the overlapping eigenfunctions (locally) around  $e$  and the  $\langle \cdot \rangle$  is also a local average. It is to be noted that in case of the global level density:  $R_1(e) = 2N \langle \rho(e) \rangle = \sum_k \langle \delta(e - e_k) \rangle$ , the sum is over entire energy range and the  $\langle \cdot \rangle$  over  $\delta$  is local around energy  $e$ . Therefore,

$$\langle \rho_{loc}(e) \rangle = \frac{\zeta}{2N} R_1(e) \quad (17)$$

where  $\zeta$  is the correlation volume of eigenstates and  $2N$  is the size of the Hamiltonian matrix  $H$ . The range of the value of  $\zeta$  is as follows: for delocalized eigenstates  $\zeta = 2N$  and for extremely localized case  $\zeta = 1$ <sup>1</sup>. Therefore,  $\langle \rho_{loc}(e) \rangle$  changes from  $\frac{1}{2N} R_1(e)$  to  $R_1(e)$  as we go from localized to delocalized eigenstates, *i.e.*  $\frac{1}{2N} R_1(e) < \langle \rho_{loc}(e) \rangle < R_1(e)$ . Eq. 15 can be written as

$$\Lambda(e, Y) = (Y - Y_0) \left( \frac{\zeta R_1(e)}{2N} \right)^2. \quad (18)$$

This rescaled complexity parameter not only have the information about different parameters (mean and variance in case of Gaussian distribution) of the distribution but also depends on density and the localization properties of the spectrum at the point of interest  $e$ .

## 4 Details of different ensembles with same matrix constraints

In this section, we present the details of the different ensembles arising due to different ensemble constraints despite preserving same matrix constraint. Depending on the choice of the form of variance in Eq. 9 which serves the purpose of ensemble constraint

---

<sup>1</sup>Note that, here one can expect  $\zeta$  to be equal to the participation ratio. (*i.e.*  $\zeta = \frac{1}{\langle I_2(e) \rangle}$ ), but this is not true if the inverse participation ratio (IPR)  $I_2(e)$  varies with energy  $e$ .

here, we study three ensembles (a) Brownian (b) Anderson and (c) exponential ensemble. All these three ensembles have the particle-hole, time-reversal and spin rotation symmetry.

#### 4.1 Brownian ensemble (BE)

The evolution of a stationary ensemble under perturbation from one stationary limit to another can be described by Brownian motion model [35]. The non-stationary intermediate states of diffusion connecting two equilibrium ensembles at both ends can be represented by a Brownian ensemble [7]. The initial integrable individual blocks of  $H$  in Eq. 5 under the basis-independent Gaussian perturbation can transit to chaotic limit preserving all the symmetries imposed on  $H$ . The variance and mean of the matrix elements distribution in Eq. 9 are chosen to be

$$h_{kk} = h_{k,N+k} = \frac{1}{2\gamma} \quad (19)$$

$$h_{kl} = h_{k,N+l} = \frac{h_{kk}}{2(1+\mu)} \quad (20)$$

$$b_{kl} = b_{k,N+l} = 0 \quad \forall k, l. \quad (21)$$

Here  $\mu \equiv cN^2$  with  $N$  as the dimension of  $\mathcal{H}$  (which is also the dimension of  $\Delta$ ) and  $c$  is an arbitrary parameter. Zero-mean of the Gaussian random variable ensures each block of  $H$  to be diagonal in  $c \rightarrow \infty$  limit, while renders GOE behavior in  $c \rightarrow 0$  limit. The ensemble density (Eq. 9) in these parameters takes the form,

$$\rho(H, h, b) = \mathcal{C} \exp \left[ -\gamma \sum_k H_{kk}^2 - 2\gamma(1+\mu) \sum_{k<l=1}^N |H_{kl}|^2 - \gamma \sum_k H_{k,N+k}^2 - 2\gamma(1+\mu) \sum_{k<l=1}^N |H_{k,N+l}|^2 \right] \mathcal{F}_s, \quad (22)$$

while the complexity parameter (Eq. 14) will become

$$Y = \frac{N}{M\gamma} \left[ \ln(2) - \frac{N-1}{2} \ln \left\{ 1 - \frac{1}{2(1+\mu)} \right\} \right]. \quad (23)$$

For the initial density when we have zero hopping, the complexity parameter  $Y$  is  $Y_0 = \frac{N}{M\gamma} \ln(2)$ . Subtracting this initial  $Y_0$  from  $Y$  and putting the number of non-zero independent elements  $M = N(N+1)/2$ ,

$$Y - Y_0 = -\frac{(N-1)}{\gamma(N+1)} \ln \left\{ 1 - \frac{1}{2(1+\mu)} \right\}. \quad (24)$$

Expanding the logarithm (ignoring the higher order terms), in the limit  $N \gg 1, \mu \gg 1$ , we obtain

$$Y - Y_0 \simeq \frac{1}{2\gamma\mu}. \quad (25)$$

In case of Brownian ensemble, the eigenfunctions are delocalized over entire Hilbert space [6, 7] leading the correlation volume  $\zeta$  in Eq. 18 to be equal to the matrix size  $2N$ . Therefore, the rescaled complexity parameter  $\Lambda$  in this case is given by

$$\Lambda_B(e, Y) = (Y - Y_0)R_1(e)^2 \quad (26)$$

with  $Y - Y_0$  provided in Eq. 25. Throughout this paper, we have considered the numerical value of the arbitrary parameter  $\gamma$  in the definition of  $Y$  in Eq. 14 to be equal to  $1/4$ . Now substituting the values of  $\gamma$  and  $\mu$ , we have

$$\Lambda_B(e) = \frac{2}{cN^2}R_1(e)^2. \quad (27)$$

In all the calculation,  $c$  is the true free parameter for this ensemble.

## 4.2 Anderson Ensemble (AE)

Transport properties of a conduction band electron in presence of impurities was first studied by Anderson by writing down a tight-binding model with nearest neighbor interaction [36]. The ensemble of such random Hamiltonians are often referred as Anderson ensemble [7]. The dimension of the system decides the number of nearest neighbors and accordingly determines the sparsity of the Hamiltonian matrix in site basis. Here, the individual blocks in  $H$  in Eq. 5 represent 2D Anderson ensemble and the variances and mean of their elements in Eq. 9 are taken as

$$h_{kk} = h_{k, N+k} = \frac{w^2}{12}, \quad b_{kk} = 0 \quad (28)$$

$$h_{kl} = h_{k, N+l} = f_1(k, l) \frac{w_s^2}{12}, \quad b_{kl} = b_{k, N+l} = f_2(k, l)t_s \quad (29)$$

with  $f_1(k, l)$  and  $f_2(k, l)$  are equals to 1 for connected sites on a two dimensional lattice and otherwise zero,  $w$  and  $w_s$  are arbitrary parameters. Here we consider  $t_s = 0$ , so that mean of the hopping elements distribution becomes zero. All the mean of the distribution are taken to be zero, so that the sparsity of the Hamiltonian matrix can be controlled by variances only. Keeping  $w_s$  fixed and varying  $w$  from  $\sim w_s$  to higher value leads the eigenstates of  $H$  from delocalized to localized ones. The ensemble density (Eq. 9) in this case is,

$$\rho(H, h, b) = \mathcal{C} \exp \left[ -\frac{6}{w^2} \sum_{k=1}^N H_{kk}^2 - \frac{6}{w_s^2} \sum_{k < l=1}^N \frac{1}{f_1(k, l)} |H_{kl}|^2 - \frac{6}{w^2} \sum_{k=1}^N H_{k, N+k}^2 - \frac{6}{w_s^2} \sum_{k < l=1}^N \frac{1}{f_1(k, l)} |H_{k, N+l}|^2 \right] \mathcal{F}_s, \quad (30)$$

while the complexity parameter from Eq. 14 becomes

$$Y = -\frac{N}{M\gamma} \left[ \ln \left| 1 - \gamma \frac{w^2}{12} \right| + \frac{z}{2} \ln \left| 1 - \gamma \frac{w_s^2}{6} \right| \right] + Y_0, \quad (31)$$

where  $z$  is the number of nearest neighbor (non-zero) elements for each row of the matrix.  $Y_0$  is the initial complexity parameter.

For all the numerical work, we consider two dimensional Anderson Hamiltonian *i.e.*  $z = 4$ . We have chosen the variances of the off-diagonal elements of block matrices as  $w_s^2 = 12$  which fixes the hopping parameter. Substituting these values along with that of  $\gamma (= 1/4)$ , we get

$$Y - Y_0 = -\frac{4}{N+1} \ln \left| 1 - \frac{w^2}{48} \right| + \frac{8}{N+1} \ln(2) \quad (32)$$

with the number of non-zero independent elements  $M = N(N+1)$ . Here the free parameter is  $w^2$ .

The correlation volume  $\zeta$  in Eq. 18 is taken intuitively as participation ratio, *i.e.*  $\zeta = \frac{1}{\langle I_2(e) \rangle}$ , with  $\langle \cdot \rangle$  to be ensemble average of the local average around energy  $e$ . The re-scaled complexity parameter in this case is given by

$$\Lambda_A(e, Y) = (Y - Y_0) \left( \frac{R_1(e)}{2N \langle I_2(e) \rangle} \right)^2 \quad (33)$$

where  $(Y - Y_0)$  is provided in Eq. 32.

### 4.3 Ensemble with exponential decay (EE)

A random band matrix model when no longer bounded by nearest neighbor interactions becomes less sparse. Considering the hopping is random and the variances of this Gaussian random hopping decay with the increasing distances between two adjacent lattice sites, one of the possible ways to model such system is exponential ensemble (introduced in [37]). Here, the block matrices of  $H$  in Eq. 5 belong to exponential ensemble where the variances of their matrix elements distribution show exponential decay from their diagonals [6]. The exponential suppressed variances in Eq. 9 are given

by

$$h_{kl} = h_{k,N+l} = \frac{1}{\exp\left(\frac{|k-l|}{\tilde{b}}\right)^2} \quad (34)$$

where  $\tilde{b}$  is an arbitrary parameter. As  $\tilde{b} \rightarrow \infty$ , the Hamiltonian becomes completely chaotic whereas decreasing finite value of  $\tilde{b}$ , localizes the system. At initial state when no hopping is introduced, *i.e.* at  $\tilde{b} \rightarrow 0$ , individual blocks of  $H$  are integrable since the mean of the distribution is chosen to be  $b_{kl} = b_{k,N+l} = 0$  for all  $k$  and  $l$ . The sparsity as well as the structure of the Hamiltonian matrix  $H$  can be determined by tuning only the parameter  $\tilde{b}$ . The probability distribution (Eq. 9) of this ensemble becomes

$$\begin{aligned} \rho(H, h, b) = \mathcal{C} \exp \left[ -\frac{1}{2} \sum_k H_{kk}^2 - \sum_{k < l=1}^N \frac{\exp\left(\frac{|k-l|}{\tilde{b}}\right)^2}{2} |H_{kl}|^2 \right. \\ \left. - \frac{1}{2} \sum_k H_{k,N+k}^2 - \sum_{k < l=1}^N \frac{\exp\left(\frac{|k-l|}{\tilde{b}}\right)^2}{2} |H_{k,N+l}|^2 \right] \mathcal{F}_s. \end{aligned} \quad (35)$$

The complexity parameter  $Y$  from Eq. 14 takes the form

$$Y = -\frac{1}{M\gamma} \left[ N \ln(1 - \gamma) + \sum_{r=1}^{N-1} (N - r) \ln \left| 1 - \frac{2\gamma}{\exp\left(\frac{r}{\tilde{b}}\right)^2} \right| \right] \quad (36)$$

with  $r \equiv |k - l|$ . Subtracting initial state complexity  $Y_0 = -\frac{N}{M\gamma} \ln(1 - \gamma)$  yields

$$Y - Y_0 = -\frac{8}{N(N+1)} \sum_{r=1}^{N-1} (N - r) \ln \left| 1 - \frac{1}{2 \exp\left(\frac{r}{\tilde{b}}\right)^2} \right| \quad (37)$$

with the number of non-zero independent matrix elements  $M$  as equal to  $\frac{N(N+1)}{2}$  and  $\gamma = 1/4$ . The free parameter is  $\tilde{b}$ .

In this ensemble, the correlation volume  $\zeta$  in Eq. 18 is considered as  $\zeta = \frac{1}{N^{1/4} \langle I_2(e) \rangle}$ , the re-scaled complexity parameter  $\Lambda$  is now given by

$$\Lambda_E(e, Y) = (Y - Y_0) \left( \frac{R_1(e)}{2N \times N^{1/4} \langle I_2(e) \rangle} \right)^2 \quad (38)$$

with  $(Y - Y_0)$  described as in Eq. 37.

## 5 Transition from Poisson to Wigner-Dyson statistics in single spectrum: universality

Coming to first of the two questions we posed in introduction about the behavior of spectral statistics as a function of energy, we choose to study short range correlations,

namely, ratio of nearest neighbor spacing distribution. First, to understand the spectral properties of particle-hole symmetric ensembles, let's recall the discussion in Ref. [5] briefly. The joint probability distribution function of eigenvalues of the CI variant of particle-hole symmetric Hamiltonian is given by,

$$P(\{e\}) d\{e\} \propto \prod_{i < j}^{2N} |e_i^2 - e_j^2| \prod_k^{2N} |e_k| \exp^{-e_k^2/h^2} de_k \quad (39)$$

where  $|e_k|$  represents the absence of energy eigenvalues at origin which is attributed to the interaction of  $k$ th level  $e_k$  with its “image”  $-e_k$ . The term  $|e_i^2 - e_j^2|$  describes mutual repulsion between levels and the factor  $(e_i + e_j)$  in  $|e_i^2 - e_j^2|$  is due to the interaction of  $e_i$ th level with the “image” of  $e_j$ th level. Now, to study the spectral fluctuation in terms of nearest neighbor spacing ratio, we consider the symmetry reduced spectrum by choosing positive eigenlevels only. And in the absence of “image” of  $e$ 's, according to above discussion the relevant spacing distribution will be Wigner-Dyson (see Appendix A for an illustrative calculation).

The numerical diagonalization of matrices are done using LAPACK (a standard software library for numerical linear algebra subroutines for complex matrices <sup>2</sup>) subroutines. The numerical parameters chosen for this study is detailed as follows. Throughout our analysis, we have considered  $N \times N$  block matrices for  $2N \times 2N$  Hamiltonian  $H$ . The mean ( $\{b_{kl}\}$ ) of the Gaussian distribution for all the cases is considered to be zero to keep our numerical study simple. The numerical value of the arbitrary parameter  $\gamma$  in the definition of  $Y$  in Eq. 14 is fixed to be equal to 1/4. Ensemble specific details are: **(BE)** This ensemble of matrices are exactly diagonalized for two  $c$  values ( $c = 0.4$  and 1), while  $2N = 1024$  and the size of the ensemble is taken 5000. **(AE)** Two dimensional (2D) Anderson ensemble is considered for each block matrices ( $\mathcal{H}$  and  $\Delta$ ) of the Hamiltonian in Eq. 5 with linear size  $L = 22$  and therefore, the size of  $H$  becomes  $2N = 2 \times L^2 = 968$ . An ensemble of 5000 matrices of this size is considered to diagonalize for each cases with  $w^2 = 12$  and 36 in the variance of the diagonal elements of the block matrices in Eq. 28. For all the cases the variance of the off-diagonal elements are fixed at  $w_s^2 = 12$  and the mean of the distribution are kept to be zero (*i.e.*  $t = t_s = 0$ ). **(EE)** We have considered two different cases with  $\tilde{b} = 10$  and 12 and generated 5000 matrices of size  $2N = 1024$  for both the cases for exact diagonalization.

The effect of variances, *i.e.* ensemble constraint on the spectrum despite coming from same matrix constraint when looked at as a function of energy is observed by studying the density of states (see the details in Appendix B). To explore this ensemble constraint dependence further, we look at the energy dependence of eigenstates properties as well like inverse participation ratio (IPR). The IPR is defined as the inverse of the number of basis states participating in the wavefunction. The inverse participation ratio for the  $n^{th}$  eigenstate  $\psi_n$  corresponding to the eigenvalue  $e_n$ , can be expressed as  $I_2(\psi_n) = \sum_{k=1}^{2N} |\psi_{kn}|^4$  which is second order moment of local intensity

---

<sup>2</sup>The LAPACK subroutines used for diagonalization of complex matrices are available at <https://www.netlib.org/lapack>

[1, 2, 38]. Figure 1 shows the variation of ensemble averaged IPR,  $\langle I_2(e) \rangle$ , throughout the spectrum for different ensembles. This turns out not only system-dependent but also sensitive to the numerical values of the variances of the matrix elements distribution *i.e.* again strongly depending on ensemble constraints. IPR corroborates the belief of Poisson like behavior (*i.e.* localized eigenfunctions) at the edges while more delocalized eigenfunctions in the bulk of the spectrum. The rescaled complexity parameter  $\Lambda$  as we introduced in earlier section is also strongly dependent on the local spectral energy range as well as the ensemble constraints which is clear from its definition (Eq. 15) (also see Appendix C).

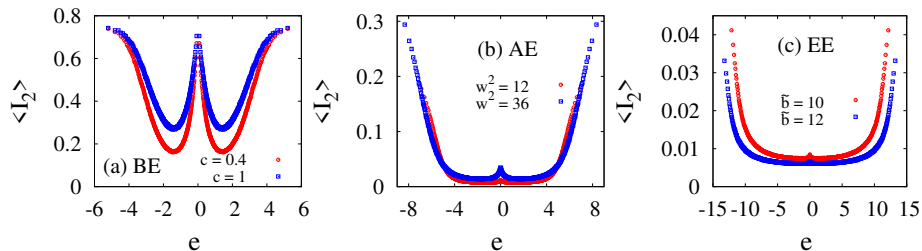


**Fig. 1:**  $\langle I_2 \rangle$  vs  $e$  for (a) BE, (b) AE and (c) EE for two different variances at each case. The  $\langle I_2 \rangle$  is sensitive to the variances of the individual ensembles as well as the type of the ensembles.

Among various spectral fluctuation measures, ratio of nearest neighbor spacing has gained a lot of popularity due to its insensitivity to the otherwise difficult procedure of unfolding [39–42]. It is defined as,

$$r_i = s_{i+1}/s_i \quad (40)$$

where  $s_i = e_{i+1} - e_i$  is the distance between two consecutive eigenvalues and the distribution of  $r$  can be denoted as

$$P(r) = \sum_i \langle \delta(r - r_i) \rangle \quad (41)$$

For the spectral statistics in the Poisson and Wigner-Dyson limit,  $P(r)$  can be given as

$$P(r) = \begin{cases} \frac{1}{(1+r)^2} & \text{for Poisson} \\ \frac{27}{8} \frac{(r+r^2)}{(1+r+r^2)^{(5/2)}} & \text{for GOE.} \end{cases} \quad (42)$$

We plot  $P(r)$  at three arbitrarily chosen values of rescaled complexity parameter  $\Lambda$  for all the three type of ensembles with two different choices of variances for each case in figure 2. The energy ranges are different for different cases. The plot shows

an universal behavior of nearest neighbor spacing distribution for different ensemble constraints as well as for different type of ensemble with same matrix constraints. Another important result here to notice is that with the increasing numerical value of  $\Lambda$ , the statistics shifts to more chaotic side while a comparatively smaller value of  $\Lambda$  showing statistics near Poissonian behavior. This motivated us to study the spectral behavior across the range of rescaled complexity parameter  $\Lambda$ .

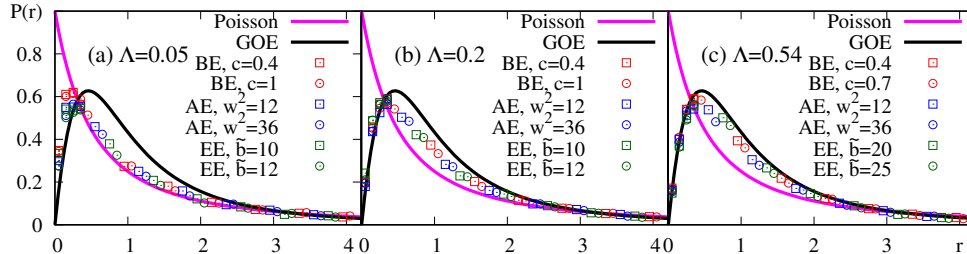


**Fig. 2:**  $P(r)$  compared for all the three ensembles for two different variances considered in each case together. Almost overlap of the curves verifies universality based on  $\Lambda$ .

We can see from Eq. 40 that  $r_i$  is an unbounded variable. Therefore, we use a related measure  $\tilde{r}_i$  defined as,

$$\tilde{r}_i = \min\left(r_i, \frac{1}{r_i}\right). \quad (43)$$

The limiting values of ensemble averaged  $\tilde{r}_i$ , denoted henceforth by  $\langle \tilde{r}_i \rangle$  for integrable and chaotic systems are as follows [40]:

$$\langle \tilde{r}_i \rangle = \begin{cases} 2 \ln(2) - 1 \approx 0.3863 & \text{for Poisson} \\ 4 - 2\sqrt{3} \approx 0.5359 & \text{for GOE.} \end{cases} \quad (44)$$

We study energy resolved  $\langle \tilde{r}_i \rangle$  to bring a fore the energy dependence of nature of spectrum. Figure 3 depicts the variation of  $\langle \tilde{r}_i \rangle$  as a function of  $\log(e_i)$  where  $e_i$  varies from center to the edge of the spectrum since it is sufficient to consider either half of the spectrum due to particle-hole symmetry. For different ensembles, the variation of  $\langle \tilde{r}_i \rangle$  is different and also with the change of the value of the variance of the matrix elements distribution, dependence of  $\langle \tilde{r}_i \rangle$  on the energy changes. Commensurate with the general belief, edge is behaving more like an integrable spectrum while bulk is similar to chaotic despite choosing a purely chaotic ensemble. But what is more interesting is the dependence on the variances *i.e.* ensemble constraints. The effect of ensemble constraint on the spectrum is clear from density of states plots along with ratio of nearest neighbor spacing plot and this effect on the eigenstates is prominent from IPR plots.

The localized and delocalized behavior at different energy range for both the ratio of spacing *i.e.* eigenvalues property and IPR which is an eigenfunction property brings

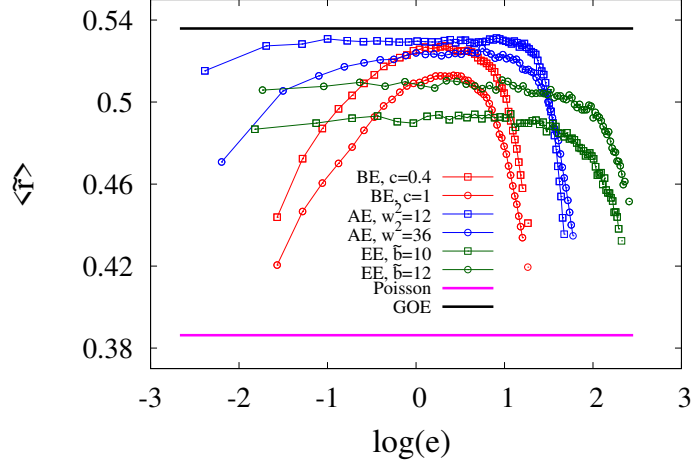


**Fig. 3:**  $\langle \tilde{r}_i \rangle$  with respect to  $\log(e_i)$  (for  $e_i > 0$ ) for (a) BE, (b) AE and (c) EE for two different variances considered in each case. The behavior is strongly system-dependent and sensitive to the value of the variances as well.

us naturally to the question whether a transition from Poisson to Wigner like behavior can be studied in a more unified manner combining the effects of spectrum as well as the ensemble constraints?

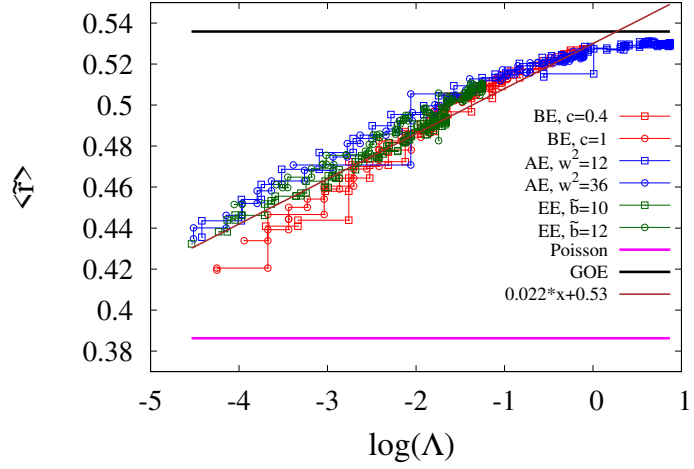


**Fig. 4:** Dependence of  $\langle \tilde{r}_i \rangle$  on  $\Lambda(e_i)$  compared for all the three ensembles for two different variances considered in each case together.  $\langle \tilde{r}_i \rangle$  is almost system independent verifying universality based on  $\Lambda$ .

To answer this question we plotted the ensemble averaged ratio of nearest neighbor spacing against the rescaled complexity parameter. It shows an universal transition from Poisson to Wigner-Dyson like behavior as seen in figure 4. Universality here is meant for not only the different ensemble constraints, but also the different type of ensembles keeping the matrix constraint same. This transition is clearly logarithmic in re-scaled complexity parameter  $\Lambda$  and  $\langle \tilde{r}_i \rangle$  saturates after a certain value of  $\Lambda$ . Previous studies for systems with and without chiral symmetry [6, 7] show this universality of the complexity parameter. Our results for different ensembles with particle-hole symmetry enforces further the universal behavior of  $\Lambda$ . However, lack of the detailed knowledge of exact dependence of  $\Lambda$  on the localization of eigenstates (depicted through  $\zeta$  in the definition of  $\Lambda$  (Eq. 18) is most probably the reason for the slight deviation of  $\langle \tilde{r}_i \rangle$  from each other in figure 4).

## 6 Interpolating ensemble from particle-hole to chiral symmetry

Motivated by the universality found in previous section and logarithmic dependence of  $\langle \tilde{r} \rangle$  on  $\Lambda$ , we introduce an interpolating ensemble which connects a system with particle-hole symmetry to one with chiral symmetry. Let us recall that in case of chiral symmetric Hamiltonian the diagonal blocks in Eq. 5 are zero matrices of appropriate dimension.

Previously, transition from Poisson to GOE [43–47], appearance of partial transport barriers in transport [43, 48], perturbation of integrable dynamical system [43, 49], in the coupled chaotic systems[50], effect of disorder strength in Anderson model[10]; GOE to GUE transition [51, 52] all have been studied in the framework of dynamical symmetry breaking in various interpolating ensembles. In contrast to this, here we are interested in Poisson to GOE transition of spectral fluctuations within a single spectrum for each instance of interpolating ensembles.

The interpolating Hamiltonian is defined as

$$H_{inter} = \begin{pmatrix} \epsilon \mathcal{H} & \Delta \\ \Delta & -\epsilon \mathcal{H} \end{pmatrix} \quad (45)$$

where  $\epsilon \in [0, 1]$  is the interpolating parameter defining the chiral symmetric and particle-hole symmetric systems at the end points. As the matrix elements are chosen as Gaussian distributed with zero mean and unit variance, multiplication of  $\epsilon$  scales the variance of diagonal block elements by  $\epsilon^2$ . We take  $\epsilon = 1, 10^{-1}, 10^{-2}, 0$  as the representative values.  $\epsilon = 0$  leads to a system with *symmetric* chiral symmetry:

$$H_c = \begin{pmatrix} 0 & \Delta \\ \Delta & 0 \end{pmatrix} \quad (46)$$

It is symmetric because the off-diagonal blocks  $\Delta$  are individually symmetric in nature and therefore, reducing the number of independent matrix elements to  $N(N + 1)/2$  for a  $2N \times 2N$  Hamiltonian matrix  $H_c$ . Note that, in general, the  $\Delta$  blocks are not necessarily symmetric or even square for chiral systems.

Now to calculate the complexity parameter  $Y$  as well as  $\Lambda$  we again consider the three different types (BE, AE and EE) of interpolating ensembles by taking the variances of the matrix elements distribution differently.

## 6.1 Brownian ensemble

Considering the variance of the diagonal elements of  $\mathcal{H}$  to be

$$h_{kk} = \frac{\epsilon^2}{2\gamma} \quad (47)$$

and keeping the other parameters as they were in Eq. 19, 20 and 21 (for  $H$  in Eq. 5) and following the same equation of complexity parameter provided in section 4.1, we achieve

$$Y - Y_0 \simeq \frac{1}{4\gamma\mu}(1 + \epsilon^2). \quad (48)$$

The correlation volume  $\zeta$  in the definition of the rescaled complexity parameter  $\Lambda$  (Eq. 18) was considered to be same as the size ( $2N$ ) of the Hamiltonian matrix in case of Brownian ensemble in 4.1. But  $\epsilon \leq 0.1$  makes  $\zeta$  to be dependent on  $\epsilon$  as  $\zeta = 2N(1 - 5^\alpha\epsilon)$  where  $\epsilon = 10^{-\alpha}$  with  $\alpha$  to be non-zero positive integer. Therefore,  $\Lambda$  becomes

$$\Lambda_B(e, Y) = (Y - Y_0)((1 - 5^\alpha\epsilon)R_1(e))^2 \quad (49)$$

with  $(Y - Y_0)$  provided by Eq. 48.

## 6.2 Anderson ensemble

If the variance of the elements of  $\mathcal{H}$  are considered to be

$$h_{kk} = \frac{\epsilon^2 w^2}{12}, \quad h_{kl} = \epsilon^2 \frac{w_s^2}{12} \quad (k, l \text{ for nn sites}) \quad (50)$$

and the other multi-parameters are defined as they were in Eq. 28 and 29 (for  $H$  in Eq. 5), following the equation of complexity parameter provided in section 4.2, one can get

$$Y - Y_0 = -\frac{2}{N+1} \ln \left\{ \left| 1 - \frac{w^2}{48} \right| \left| 1 - \frac{\epsilon^2 w^2}{48} \right| \right\} - \frac{4}{N+1} \ln \left\{ \frac{1}{2} \left( 1 - \frac{\epsilon^2}{2} \right) \right\} \quad (51)$$

The correlation volume  $\zeta$  here consists of IPR as discussed in section 4.2 which takes care the effect of  $\epsilon$  on the localization of wavefunctions. The rescaled complexity parameter  $\Lambda$ , therefore, will be same as defined in Eq. 33 with  $(Y - Y_0)$  given by Eq. 51.

### 6.3 Ensemble with exponential decay

The variance of the elements of  $\mathcal{H}$  for EE is given by

$$h_{kl} = \frac{\epsilon^2}{\exp\left(\frac{|k-l|}{b}\right)^2} \quad (52)$$

for  $k, l = 1 \rightarrow N$  and the variances of the other elements distribution are given by Eq. 34 (for  $H$  in Eq. 5) with the mean of all elements distribution to be zero. To calculate the complexity parameter, if we follow the equation provided in section 4.3, we get

$$Y - Y_0 = -\frac{4}{N(N+1)} \sum_{r=1}^{N-1} (N-r) \ln \left\{ \left| 1 - \frac{1}{2 \exp\left(\frac{r}{b}\right)^2} \right| \left| 1 - \frac{\epsilon^2}{2 \exp\left(\frac{r}{b}\right)^2} \right| \right\}. \quad (53)$$

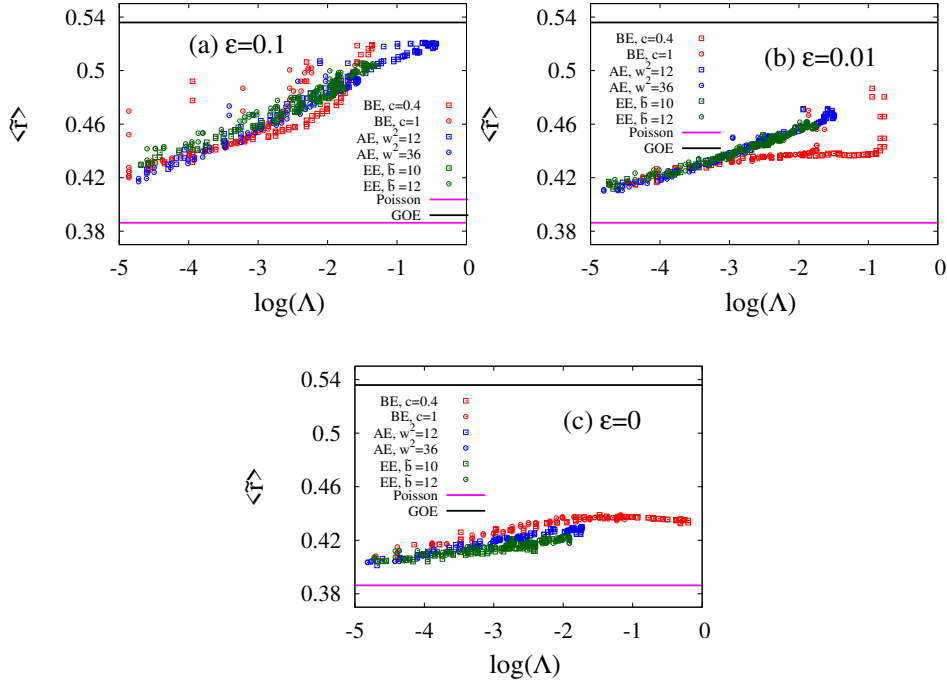


**Fig. 5:**  $\langle \tilde{r}_i \rangle$  vs  $\log(\Lambda)$  plot for (a)  $\epsilon = 10^{-1}$ , (b)  $\epsilon = 10^{-2}$  and (c)  $\epsilon = 0$ . The  $\langle \tilde{r}_i \rangle$  for different variances of same type of ensembles as well as for different ensembles coincide with each other during the transition from Poisson  $\rightarrow$  GOE before they saturate. As the value of the parameter  $\epsilon$  decreases (*i.e.* goes towards chiral ensemble from particle-hole one),  $\langle \tilde{r}_i \rangle$  saturates faster for all the cases.

In this case,  $\zeta$  is again a function of IPR provided in section 4.3 and hence, not explicitly dependent on  $\epsilon$  which keeps the definition of the  $\Lambda$  as it was defined in Eq. 38 with  $(Y - Y_0)$  to be as Eq. 53.

The variation of  $\langle \tilde{r}_i \rangle$  with  $\Lambda$  for different  $\epsilon$  as well as for different ensembles is shown in figure 5. For  $\epsilon = 0$ , the system goes away from the integrability as a function of  $\log(\Lambda)$  but saturates before it reaches to chaotic limit. This incomplete transition can be attributed to lack of sufficient independent elements in the Hamiltonian due to added symmetric nature of off-diagonal blocks. During transition, the independence on ensemble constraint once again displays the universal nature of the transition within the spectrum. With increasing value of  $\epsilon$ , complete transition happens and the universality in the independence of ensemble constraint as well as the variation of  $\langle \tilde{r} \rangle \propto \log(\Lambda)$  is maintained.

## 7 Application to 2D SSH model

In this section, we explore this universality for a physical example of 2D SSH like model once with chiral symmetry and again with particle-hole symmetry. This two dimensional generalization of 1D SSH model is a representation of bipartite lattice structure where the interaction strength inside and outside of the unit cell are considered to be different from each other. Figure 6 is a diagrammatic representation of the details of the model where two sublattices A and B having  $a_{11}, a_{21}, a_{31}, \dots, c_{11}, c_{21}, c_{31}, \dots$  and  $b_{11}, b_{21}, b_{31}, \dots, d_{11}, d_{21}, d_{31}, \dots$  lattice points respectively are shown along with the unit cell which consists of four lattice points (one of each  $a, b, c$  and  $d$ ). The pair of lattice points belonging to the same sublattice (( $a$  and  $c$ ) or ( $b$  and  $d$ )) sit at the ends of the diagonal of a square unit cell.

### 7.1 2D SSH model with chiral symmetry

Bipartite nature of the SSH model makes the nearest neighbors (both inside and outside of the unit cell) of every lattice point to belong to the other sublattice. Only nearest neighbor interactions are being considered in this representation of 2D SSH model with chiral symmetry [Left figure of Fig. 6]. Here the interaction between the lattice points belonging to same sublattice are forbidden. The interaction strength inside and outside of the unit cell are taken different from each other  $\alpha$  and  $\alpha'$  respectively. The interaction Hamiltonian of this model looks like

$$H_S^{ch} = \sum_{x,y=1}^{L/2} \left[ \alpha_{xy}^{ab} a_{xy}^\dagger b_{xy} + \alpha_{xy}^{cd} c_{xy}^\dagger d_{xy} + \alpha_{xy}^{da} d_{xy}^\dagger a_{xy} + \alpha_{xy}^{bc} b_{xy}^\dagger c_{xy} \right. \\ \left. \alpha_{xy}^{ba} b_{xy}^\dagger a_{x+1,y} + \alpha_{xy}^{cd} c_{xy}^\dagger d_{x+1,y} + \alpha_{xy}^{da} d_{xy}^\dagger a_{x+1,y} + \alpha_{xy}^{cb} c_{xy}^\dagger b_{x+1,y} \right] \quad (54)$$

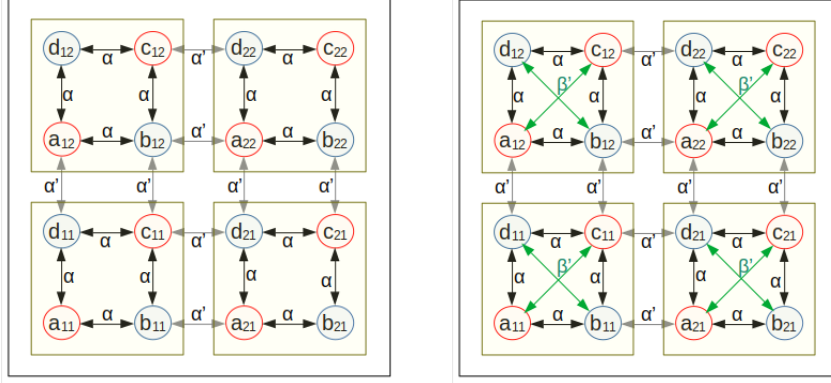


**Fig. 6:** A 2D SSH model for lattice size  $L = 4$  is shown here. The *red* and the *blue* lattice points represent their associated sublattices to be different from each other. The *yellow* squares represent each unit cell consisting four lattice points; two from each sublattice. The *black* arrows represent interaction between two lattice points belonging to different sublattice inside ( $\alpha$ ) the unit cells whereas the *grey* ones represent that outside ( $\alpha'$ ) the unit cells. Left figure is for 2D SSH model with chiral symmetry and the right one is that with particle-hole symmetry. The latter one also consists diagonal interactions within the same unit cell represented by *green* arrows.

with  $L$  being the lattice size. The Hamiltonian  $H_S^{ch}$  can be expressed as  $H_S^{ch} = \psi^\dagger H_{SSH}^{ch} \psi$  with

$$H_{SSH}^{ch} = \begin{pmatrix} 0 & \Delta \\ \Delta^T & 0 \end{pmatrix} \quad (55)$$

in site basis  $\psi^\dagger = (a_{11}^\dagger, a_{21}^\dagger, \dots, c_{11}^\dagger, c_{21}^\dagger, \dots, b_{11}^\dagger, b_{21}^\dagger, \dots, d_{11}^\dagger, d_{21}^\dagger, \dots)$ . Here, the off diagonal block matrix  $\Delta$  is of size  $N \times N$  for  $H_{SSH}^{ch}$  of size  $2N = L^2$ . The  $H_{SSH}^{ch}$  is a representation of systems with chiral symmetry where the off-diagonal blocks are not symmetric. The energy spectrum in this case like particle-hole symmetric system is symmetric around zero.

For numerical analysis of spectral statistics, we have considered an ensemble of 500 matrices of 2D lattice of size  $L = 32$ . We defined the interaction strengths inside and outside ( $\alpha$  and  $\alpha'$  respectively) of the unit cell as Gaussian distributed random number to model the disorder. The mean and variance are the relevant parameters for the present study. Here we have considered three combinations of the variances  $h_\alpha$  and  $h_{\alpha'}$ : i)  $h_\alpha = 1, h_{\alpha'} = 3/2$ , ii)  $h_\alpha = 3/2, h_{\alpha'} = 1$  and iii)  $h_\alpha = 3, h_{\alpha'} = 1$  once with zero mean of the matrix elements and at other time with non-zero mean  $b_\alpha = 0.2, b_{\alpha'} = 0.1$ . The density of states is symmetric around zero energy as expected due to chiral symmetry. The level density depends on the sum of the variances of interaction strengths inside and outside of the unit cell. The width of the spectrum increases with the increasing value of  $h_\alpha + h_{\alpha'}$  while IPR  $\langle I_2 \rangle$  depends on the sum as well as the modulus difference between  $h_\alpha$  and  $h_{\alpha'}$ . For a fixed value of  $|h_\alpha - h_{\alpha'}|$ , with increasing value of  $h_\alpha + h_{\alpha'}$ , the eigenstates tend to delocalize. However, for a

fixed sum, localization increases with increasing  $|h_\alpha - h_{\alpha'}|$  which is understandable as the strength of the disorder become at par inside and outside the unit cell.

Following the definition of the complexity parameter provided in Eq. 14, the  $Y$  in this case is given by

$$Y = -\frac{1}{2M\gamma} \left[ N \ln |1 - \gamma h_\alpha| + N \ln |1 - 2\gamma h_\alpha| + 2N \ln |1 - 2\gamma h_{\alpha'}| \right. \\ \left. + 2N \ln |b_\alpha|^2 + 2N \ln |b_{\alpha'}|^2 \right] + Y_0 \quad (56)$$

where  $M$  is the number of non-zero independent matrix elements,  $\gamma$  is an arbitrary parameter considered to be equals to  $1/4$  throughout while  $Y_0$  is the complexity parameter of the initial state which corresponds to the Poisson limit attained by the system. For our calculation, we have chosen interaction inside the unit cell much higher ( $h_\alpha = 9$ ) than that at outside ( $h_{\alpha'} = 0.01$ ) for this limit. In total eight logarithmic terms appear as we consider two dimensional system resulting in the number of the nearest neighbor elements to be four. Considering  $M = N(N + 1)/2$  and the correlation volume  $\zeta$  to be equal to the participation ratio (*i.e.*  $\zeta = \frac{1}{\langle I_2 \rangle}$ ), the rescaled complexity parameter  $\Lambda$  becomes same as Eq. 33, where  $Y - Y_0$  is defined by Eq. 56. The ensemble averaged ratio of nearest neighbor spacing  $\langle \tilde{r}_i \rangle$  is plotted as function of  $\log(\Lambda)$  in figure 7 for this 2D SSH model with chiral symmetry.

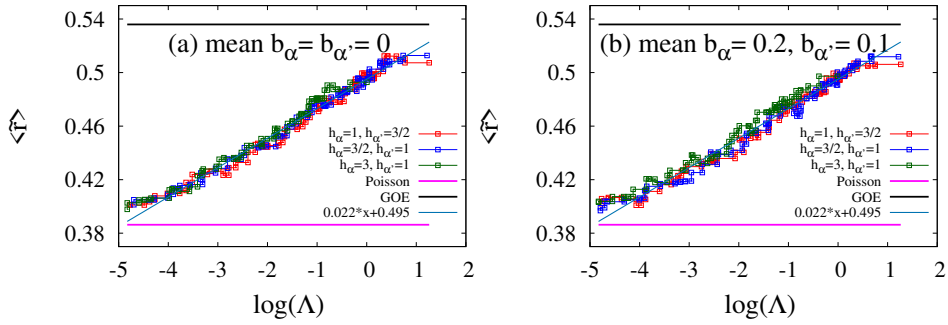


**Fig. 7:**  $\langle \tilde{r}_i \rangle$  with respect to  $\log(\Lambda(e_i))$  for 2D SSH with chiral symmetry for different distribution of the interaction strengths  $\alpha$  and  $\alpha'$ . In (a) mean of the distribution  $b_\alpha = b_{\alpha'} = 0$  whereas in (b)  $b_\alpha = 0.2, b_{\alpha'} = 0.1$ . For both the cases three different combinations of the variances are plotted. With the increasing numerical value of  $\Lambda$ , the  $\langle \tilde{r}_i \rangle$  goes from near Poisson to close to GOE limit and this transition is independent of all the ensemble constraints considered like means and variances.

It is clear from figure 7 that  $\langle \tilde{r}_i \rangle$  not only shows a transition from nearly integrable value to chaotic limit with the increase of the numerical value of  $\Lambda$  but also this transition is independent of the distribution parameters (mean and variances which are ensemble constraints), verifying universality of spectral fluctuations based on  $\Lambda$ .

The logarithmic dependence of averaged nearest neighbor spacing ratio on complexity parameter agrees well with our result described in section 5. This correspondence in first glance may look surprising as true symmetry of 2D SSH model considered here is chirality however the resolution of this is in the total number of ensemble constraints which in this case is same as in the system with particle-hole symmetry. The mean value of the matrix elements distribution does not change the logarithmic dependence of  $\langle \tilde{r}_i \rangle$  on the numerical values of  $\Lambda$ , moreover the rate with which this transition happens is independent of mean.

## 7.2 2D SSH model with CI class of particle-hole symmetry

In the particle-hole symmetric version of 2D SSH model, along with already existing interactions, we now consider onsite disorder of strength  $\beta$  for all lattice points and non-zero interaction of strength  $\beta'$  between the lattice points belonging to same sublattice only inside the unit cells (a-c and b-d) [Right figure of Fig. 6]. The interaction Hamiltonian will now become

$$H_S^{ph} = H_S^{ch} + \sum_{x,y=1}^{L/2} \left[ \beta_{xy}^{aa} a_{xy}^\dagger a_{xy} + \beta_{xy}^{bb} b_{xy}^\dagger b_{xy} + \beta_{xy}^{cc} c_{xy}^\dagger c_{xy} + \beta_{xy}^{dd} d_{xy}^\dagger d_{xy} + \beta_{xy}'^{ac} a_{xy}^\dagger c_{xy} + \beta_{xy}'^{bd} b_{xy}^\dagger d_{xy} \right] \quad (57)$$

with  $H_S^{ch}$  taken from Eq. 54. The Hamiltonian  $H_S^{ph}$  can be expressed as  $H_S^{ph} = \psi^\dagger H_{SSH}^{ph} \psi$  with  $\psi^\dagger = (a_{11}^\dagger, a_{21}^\dagger, \dots, c_{11}^\dagger, c_{21}^\dagger, \dots, b_{11}^\dagger, b_{21}^\dagger, \dots, d_{11}^\dagger, d_{21}^\dagger, \dots)$  where the Hamiltonian matrix  $H_{SSH}^{ph}$  will have non-zero diagonal blocks. It will be particle-hole symmetric of CI class, if  $H_S^{ph}$  has additional terms:  $\sum_{x,y=1}^{L/2} [\alpha_{xy}'^{ba} b_{x+1,y}^\dagger a_{xy} + \alpha_{xy}'^{cd} c_{x+1,y}^\dagger d_{xy}]$ , along with the conditions as follows

$$\alpha_{xy}^{da} = \alpha_{xy}^{bc}, \quad \alpha_{xy}'^{da} = \alpha_{xy}'^{cb}, \quad \beta_{xy}^{aa} = -\beta_{xy}^{bb}, \quad \beta_{xy}^{cc} = -\beta_{xy}^{dd} \quad \text{and} \quad \beta_{xy}'^{ac} = \beta_{xy}'^{bd}. \quad (58)$$

$H_{SSH}^{ph}$  will now exactly look like  $H$  in Eq. 5 with same number of independent ensemble constraints.

For numerical study, all the interaction strengths ( $\beta$  and  $\beta'$  along with  $\alpha$  and  $\alpha'$ ) are defined to be Gaussian distributed random numbers. Four combinations of the variances  $h_\alpha, h_{\alpha'}, h_\beta$  and  $h_{\beta'}$  are considered: i)  $h_\alpha = h_{\alpha'} = h_\beta = h_{\beta'} = 1$ , ii)  $h_\alpha = h_{\alpha'} = 1, h_\beta = h_{\beta'} = 3/2$ , iii)  $h_\alpha = h_{\alpha'} = 3/2, h_\beta = h_{\beta'} = 1$  and iv)  $h_\alpha = h_\beta = 1, h_{\alpha'} = h_{\beta'} = 3/2$  for both zero and non-zero mean  $b_\alpha = b_\beta = 0.1, b_{\alpha'} = b_{\beta'} = 0.2$ .

The complexity parameter in this case, following the definition in Eq. 14, will now become  $Y = Y_{od} + Y_d + Y_0$  with

$$Y_{od} \equiv -\frac{1}{2M\gamma} \left[ N \ln |1 - \gamma h_\alpha| + \frac{N}{2} \ln |1 - 2\gamma h_\alpha| + \frac{3N}{2} \ln |1 - 2\gamma h_{\alpha'}| + \frac{3N}{2} \ln |b_\alpha|^2 + \frac{3N}{2} \ln |b_{\alpha'}|^2 \right] \quad (59)$$

$$Y_d \equiv -\frac{1}{2M\gamma} \left[ N \ln |1 - \gamma h_\beta| + \frac{N}{2} \ln |1 - 2\gamma h_{\beta'}| + N \ln |b_\beta|^2 + \frac{N}{2} \ln |b_{\alpha'}|^2 \right] \quad (60)$$

with  $M$  and  $\gamma$  being again the number of non-zero independent matrix elements considered as  $M = N(N+1)/2$  and an arbitrary parameter to be equal to  $1/4$  respectively.  $Y_0$  is the complexity parameter at the initial state. We have chosen the onsite disorder much higher ( $h_\beta = 9$ ) than the interaction between any two lattice points ( $h_\alpha = h_{\alpha'} = h_{\beta'} = 0.01$ ) to achieve the Poisson limit by the system. Again, considering the correlation volume  $\zeta$  to be equal to the participation ratio, the rescaled complexity parameter  $\Lambda$  becomes same as Eq. 33, where  $Y - Y_0 = Y_{od} + Y_d$  with  $Y_{od}$  and  $Y_d$  being defined by Eq. 59 and Eq. 60 respectively. Figure 8 shows the ensemble averaged ratio of nearest neighbor spacing  $\langle \tilde{r} \rangle$  with respect to  $\log(\Lambda)$  for this 2D SSH model with particle-hole symmetry of CI kind. Here an ensemble of 500 matrices of 2D lattice of size  $L = 32$  is considered.

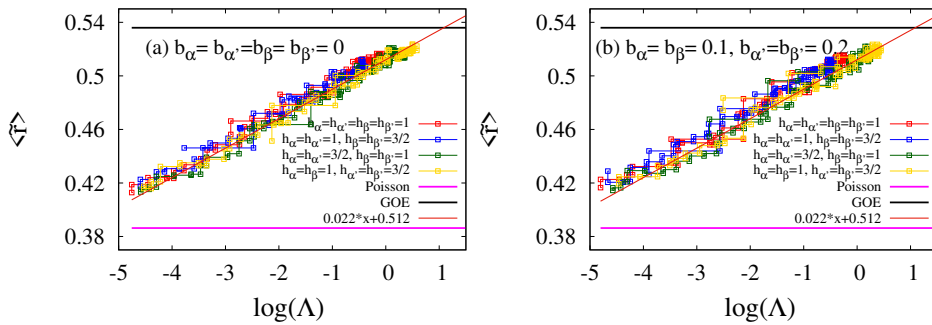


**Fig. 8:**  $\langle \tilde{r}_i \rangle$  as a function of  $\log(\Lambda(e_i))$  for 2D SSH with particle-hole symmetry for different distribution of the interaction strengths  $\alpha, \alpha', \beta$  and  $\beta'$ . In (a) mean of the distribution  $b_\alpha = b_{\alpha'} = b_\beta = b_{\beta'} = 0$  whereas in (b)  $b_\alpha = b_\beta = 0.1, b_{\alpha'} = b_{\beta'} = 0.2$ . For both the cases four different combinations of the variances are plotted. With the increasing numerical value of  $\Lambda$ , the  $\langle \tilde{r}_i \rangle$  goes from near Poisson to near GOE limit and this transition is independent of all the ensemble constraints considered like means and variances.

Figure 8 again confirms a transition of  $\langle \tilde{r}_i \rangle$  from nearly integrable value to chaotic limit with the increase of the numerical value of  $\Lambda$  and its independence of the distribution parameters like mean and variances. This result again verifies the universality of spectral fluctuations based on  $\Lambda$ . Again,  $\langle \tilde{r}_i \rangle \propto \log(\Lambda)$ . For both the 2D SSH models one with chiral symmetry and the other one with particle-hole symmetry, the rate of transition is same. Even the mean value does not change the logarithmic dependence of  $\langle \tilde{r}_i \rangle$  on the numerical values of  $\Lambda$ , as well as the rate of the transition.

## 8 Conclusions

In this paper, we have shown that the spectral statistics characterized by ensemble averaged ratio of nearest neighbor spacing shows an universal transition from integrable to chaotic behavior within single spectrum, when studied as a function of complexity parameter for the system having particle-hole symmetry. The universality here means that transition does not depend on ensemble constraints whenever the matrix constraints are kept fixed. Moreover, the  $\langle \tilde{r} \rangle$  goes as  $\log(\Lambda)$ . The complexity parameter itself is a function of different parameters present in the joint probability distribution function of the system. Introduced via diffusion equation for JPDF in the parameter space, this quantity in addition requires the local information regarding spectral density as well as localization property of eigenfunctions. The different ensembles like Brownian, Anderson and exponential show the same behavior and completely fall on top of each other as seen in figure 4.

We further have introduced and studied an interpolating ensemble having a single parameter  $\epsilon \in [0, 1]$  which gives chiral and particle-hole symmetric Hamiltonian at its end-points. We further show that for a fixed value of  $\epsilon$ , the transition from integrable to Wigner-Dyson value follows the universality and  $\langle \tilde{r} \rangle \propto \log(\Lambda)$ . Motivated by this, we studied two different 2D SSH like models one with chiral symmetry and the other one with particle-hole symmetry where bond disorder and chemical potential are modeled by Gaussian random numbers. The spectral transition within the spectrum again follows the universality for both the models with different combinations of mean and variances of the matrix elements distribution.

In our analysis we have considered the localization volume  $\zeta$  intuitively for various ensembles guided also by previous works [6, 7, 53]. A systematic study of this as a function of energy would improve this analysis on the quantitative level and can be studied in future.

## Acknowledgement

One of the authors, T. Mondal, gratefully acknowledges Professor Pragya Shukla for introducing her to the complexity parameter and educating about its universal behavior for different symmetry classes of random matrix ensemble.

## Declarations

### Authors' contributions

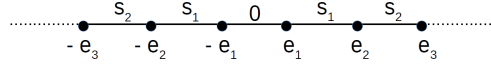
All the authors prepared the manuscript.

### Data availability statement

Data sharing not applicable to this article as no datasets were generated or analyzed during the current study.

## Appendix A Nearest neighbor spacing distribution

A particle-hole symmetric matrix have eigenvalues always symmetric around zero. Therefore, if we sort them, the spacing between  $e_i$  and  $e_{i+1}$  will be equal to the spacing between  $-e_i$  and  $-e_{i+1}$ , *i.e.*  $|e_{i+1} - e_i| = s$ .



Hence, it is sufficient to consider either side of the spectrum as long as nearest neighbor fluctuation is the spectral property of interest.

Considering Eq. 5 to be a  $4 \times 4$  Hamiltonian, two of its four eigenvalues will be positive due to particle-hole symmetry. Therefore, without any loss of generality, restricting ourselves to only positive sector of eigenvalues, we can calculate the nearest neighbor spacing distribution  $P(s)$ .

Let us assume, the two positive eigenvalues are  $e_1$  and  $e_2$  and the spacing between them is  $s$ . Therefore,

$$\begin{aligned}
 P(s) &= \int_0^\infty \int_0^\infty P(e_1, e_2) \delta(s - |e_1 - e_2|) de_1 de_2 \\
 &= \int_0^\infty de_1 \int_0^{e_1} P_{e_1 > e_2} \delta(s - |e_1 - e_2|) de_2 \\
 &\quad + \int_0^\infty de_2 \int_0^{e_2} P_{e_2 > e_1} \delta(s - |e_2 - e_1|) de_1
 \end{aligned} \tag{A1}$$

Using Eq. 39, one can write  $P(e_1, e_2)$ . Now,

$$\begin{aligned}
 P(s) &\propto \int_0^\infty de_1 \int_0^{e_1} (e_1^2 - e_2^2) e_1 e_2 \exp\left(-\frac{e_1^2 + e_2^2}{h^2}\right) \delta(s - |e_1 - e_2|) de_2 \\
 &\quad + \int_0^\infty de_2 \int_0^{e_2} (e_2^2 - e_1^2) e_1 e_2 \exp\left(-\frac{e_1^2 + e_2^2}{h^2}\right) \delta(s - |e_2 - e_1|) de_1 \\
 &= 2 \int_0^\infty de_1 (e_1^2 - (e_1 - s)^2) e_1 (e_1 - s) \exp\left(-\frac{e_1^2 + (e_1 - s)^2}{h^2}\right) \\
 &= \frac{h^4}{2} s e^{-s^2/h^2}
 \end{aligned} \tag{A2}$$

Therefore,

$$P(s) \propto s e^{-s^2/h^2}. \tag{A3}$$

This spacing distribution is same as that of GOE. Now for  $2000 \times 2000$  Hamiltonian matrix we numerically verified this analytical result.

Since our spectral property of interest is nearest neighbor spacing ratio distribution, we numerically present here  $P(r)$  and  $P(\tilde{r})$  for particle-hole CI class of random matrices with no additional constraints (Eq. 5), The distributions here agree very well with the result of Gaussian Orthogonal Ensemble (GOE).

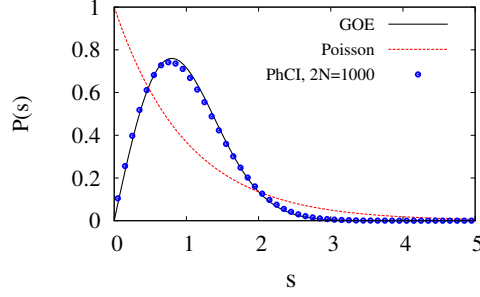


**Fig. A1:** Distribution of nearest neighbor spacing for an ensemble of 5000 Ph-CI matrices of size  $2000 \times 2000$

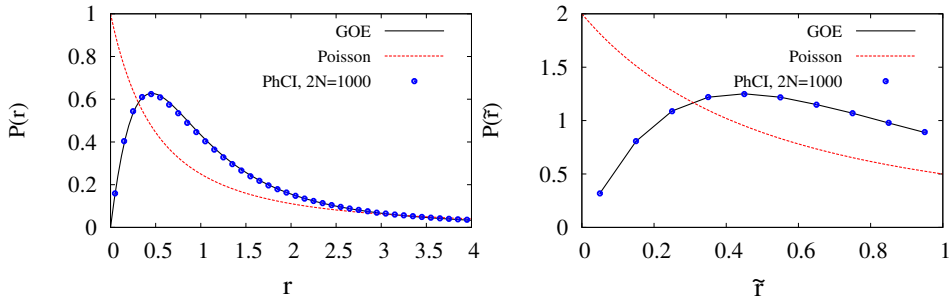


**Fig. A2:** Distribution of nearest neighbor spacing ratio of two kinds for an ensemble of 5000 Ph-CI matrices of size  $2000 \times 2000$

## Appendix B Density of states

The density of states at an energy  $e$  is given by  $\rho(e) = \sum_n \delta(e - e_n)$  [38]. The scaled level density  $F(e)$  is defined as  $F(e) = \frac{1}{2N} R_1(e)$  where  $R_1(e) = \langle \rho(e) \rangle$  due to ergodicity in the spectrum [38, 54]. Figure B3 shows that  $R_1(e)$  is dependent on the variances of the matrix elements distribution for both AE (B3(b)) and EE (B3(c)) but the dependence is insignificant for BE (B3(a)). This highlights the same finding about sensitivity to ensemble constraints despite being invariant under the same matrix constraint. The exception of BE is again commensurate with earlier findings [6]. The structure of level density curve is highly dependent on the systems obtained by varying ensemble constraints only.

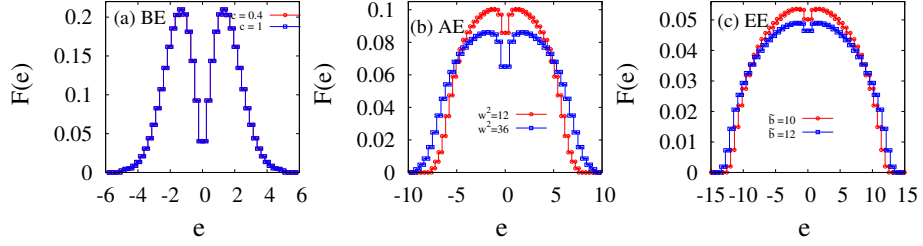


**Fig. B3:** Variance dependence of rescaled density of states  $F(e) = \frac{1}{2N}R_1(e)$  for (a) BE, (b) AE and (c) EE. The difference in level density with respect to the ensembles is very much significant.

## Appendix C Energy dependence of complexity parameter

The dependence of the rescaled complexity parameter  $\Lambda$  on the ensemble constraint variance as a function of energy for three different ensembles is shown in figure C4. The energy dependence of  $\Lambda$  is provided in its expression in Eq. 15.

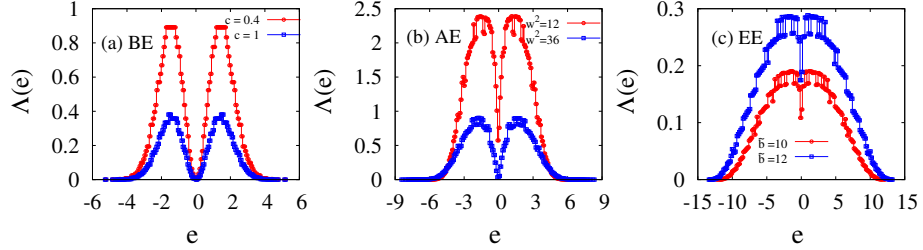


**Fig. C4:** Variation of  $\Lambda$  throughout the spectrum for (a) BE, (b) AE and (c) EE for two different variances considered in each case. The spectrum of  $\Lambda$  with respect to  $e$  is very much dependent on the variances of individual ensembles and also significantly different for different ensembles.

## References

- [1] Haake, F.: Quantum Signatures of Chaos, 3rd edn. Springer, ??? (2010)
- [2] Mehta, M.L.: Random Matrices and the Statistical Theory of Energy Levels, 2nd edn. Academic Press, Inc., New York (1991)
- [3] Shukla, P.: Generalized random matrix theory: A mathematical probe for complexity. International Journal of Modern Physics B **26**(16), 1230008 (2012)

- [4] Guhr, T., Müller–Groeling, A., Weidenmüller, H.A.: Random-matrix theories in quantum physics: common concepts. *Physics Reports* **299**(4-6), 189–425 (1998)
- [5] Altland, A., Zirnbauer, M.R.: Nonstandard symmetry classes in mesoscopic normal-superconducting hybrid structures. *Physical Review B* **55**(2), 1142 (1997)
- [6] Mondal, T., Shukla, P.: Spectral statistics of multiparametric gaussian ensembles with chiral symmetry. *Physical Review E* **102**(3), 032131 (2020)
- [7] Shukla, P.: Level statistics of anderson model of disordered systems: connection to brownian ensembles. *Journal of Physics: Condensed Matter* **17**(10), 1653 (2005)
- [8] Shukla, P.: Alternative technique for complex spectra analysis. *Physical Review E* **62**(2), 2098 (2000)
- [9] Shukla, P.: Random matrices with correlated elements: A model for disorder with interactions. *Physical Review E* **71**(2), 026226 (2005)
- [10] Evers, F., Mirlin, A.D.: Anderson transitions. *Reviews of Modern Physics* **80**(4), 1355 (2008)
- [11] Dutta, R., Shukla, P.: Complex systems with half-integer spins: symplectic ensembles. *Physical Review E* **76**(5), 051124 (2007)
- [12] Shukla, P.: Towards a common thread in complexity: an accuracy-based approach. *Journal of Physics A: Mathematical and Theoretical* **41**(30), 304023 (2008)
- [13] Andreev, A.: The thermal conductivity of the intermediate state in superconductors. *Sov. Phys. JETP* **19**(15), 1228–1231 (1964)
- [14] Shaginyan, V., Popov, K.: Asymmetric tunneling, andreev reflection and dynamic conductance spectra in strongly correlated metals. *Physics Letters A* **361**(4-5), 406–412 (2007)
- [15] Cooper, L.N.: Bound electron pairs in a degenerate fermi gas. *Physical Review* **104**(4), 1189 (1956)
- [16] Fernandes, R.M.: Lecture Notes: BCS theory of superconductivity. Unpublished (2020)
- [17] Zirnbauer, M.R.: Particle–hole symmetries in condensed matter. *Journal of Mathematical Physics* **62**(2), 021101 (2021)
- [18] Asbóth, J.K., Oroszlány, L., Pályi, A.: A short course on topological insulators. *Lecture notes in physics* **919**, 166 (2016)
- [19] Su, W., Schrieffer, J., Heeger, A.J.: Solitons in polyacetylene. *Physical review letters* **42**(25), 1698 (1979)

- [20] Heeger, A.J., Kivelson, S., Schrieffer, J., Su, W.-P.: Solitons in conducting polymers. *Reviews of Modern Physics* **60**(3), 781 (1988)
- [21] Ota, Y., Katsumi, R., Watanabe, K., Iwamoto, S., Arakawa, Y.: Topological photonic crystal nanocavity laser. *Communications Physics* **1**(1), 1–8 (2018)
- [22] Ota, Y., Liu, F., Katsumi, R., Watanabe, K., Wakabayashi, K., Arakawa, Y., Iwamoto, S.: Photonic crystal nanocavity based on a topological corner state. *Optica* **6**(6), 786–789 (2019)
- [23] Xie, B.-Y., Wang, H.-F., Wang, H.-X., Zhu, X.-Y., Jiang, J.-H., Lu, M.-H., Chen, Y.-F.: Second-order photonic topological insulator with corner states. *Physical Review B* **98**(20), 205147 (2018)
- [24] Xie, B.-Y., Su, G.-X., Wang, H.-F., Su, H., Shen, X.-P., Zhan, P., Lu, M.-H., Wang, Z.-L., Chen, Y.-F.: Visualization of higher-order topological insulating phases in two-dimensional dielectric photonic crystals. *Physical Review Letters* **122**(23), 233903 (2019)
- [25] Chen, B.-H.: Two-dimensional extended su-schrieffer-heeger model. PhD thesis, National Taiwan Normal University (Taiwan) (2018)
- [26] Chen, X.-D., Deng, W.-M., Shi, F.-L., Zhao, F.-L., Chen, M., Dong, J.-W.: Direct observation of corner states in second-order topological photonic crystal slabs. *Physical Review Letters* **122**(23), 233902 (2019)
- [27] Zheng, L.-Y., Achilleos, V., Richoux, O., Theocharis, G., Pagneux, V.: Observation of edge waves in a two-dimensional su-schrieffer-heeger acoustic network. *Physical Review Applied* **12**(3), 034014 (2019)
- [28] Kim, M., Rho, J.: Topological edge and corner states in a two-dimensional photonic su-schrieffer-heeger lattice. *Nanophotonics* **9**(10), 3227–3234 (2020)
- [29] Li, C.-A., Choi, S.-J., Zhang, S.-B., Trauzettel, B.: Tunable dirac states in a two-dimensional su-schrieffer-heeger model. arXiv preprint arXiv:2112.07697 (2021)
- [30] Li, C.-A.: Topological states in two-dimensional su-schrieffer-heeger models. *Frontiers in Physics*, 220 (2022)
- [31] BD Simons, A.A.: *Theories of mesoscopic physics*. Springer (2000)
- [32] Gnuzmann, S., Seif, B.: Universal spectral statistics in Wigner-Dyson, chiral, and Andreev star graphs. I. Construction and numerical results. *Physical Review E* **69**(5), 056219 (2004)
- [33] Gnuzmann, S., Seif, B.: Universal spectral statistics in wigner-dyson, chiral, and andreev star graphs. ii. semiclassical approach. *Physical Review E* **69**(5), 056220 (2004)

- [34] Verbaarschot, J.: Spectrum of the qcd dirac operator and chiral random matrix theory. *Physical Review Letters* **72**(16), 2531 (1994)
- [35] Dyson, F.J.: A brownian-motion model for the eigenvalues of a random matrix. *Journal of Mathematical Physics* **3**(6), 1191–1198 (1962)
- [36] Anderson, P.W.: Absence of diffusion in certain random lattices. *Physical review* **109**(5), 1492 (1958)
- [37] Fyodorov, Y.V., Mirlin, A.D.: Scaling properties of localization in random band matrices: a  $\sigma$ -model approach. *Physical review letters* **67**(18), 2405 (1991)
- [38] Brody, T.A., Flores, J., French, J.B., Mello, P., Pandey, A., Wong, S.S.: Random-matrix physics: spectrum and strength fluctuations. *Reviews of Modern Physics* **53**(3), 385 (1981)
- [39] Oganessian, V., Huse, D.A.: Localization of interacting fermions at high temperature. *Physical review b* **75**(15), 155111 (2007)
- [40] Atas, Y., Bogomolny, E., Giraud, O., Roux, G.: Distribution of the ratio of consecutive level spacings in random matrix ensembles. *Physical review letters* **110**(8), 084101 (2013)
- [41] Atas, Y., Bogomolny, E., Giraud, O., Vivo, P., Vivo, E.: Joint probability densities of level spacing ratios in random matrices. *Journal of Physics A: Mathematical and Theoretical* **46**(35), 355204 (2013)
- [42] Corps, Á.L., Relano, A.: Distribution of the ratio of consecutive level spacings for different symmetries and degrees of chaos. *Physical Review E* **101**(2), 022222 (2020)
- [43] Bohigas, O., Tomsovic, S., Ullmo, D.: Manifestations of classical phase space structures in quantum mechanics. *Physics Reports* **223**(2), 43–133 (1993)
- [44] French, J., Kota, V., Pandey, A., Tomsovic, S.: Statistical properties of many-particle spectra v. fluctuations and symmetries. *Annals of Physics* **181**(2), 198–234 (1988)
- [45] Wigner, E.P.: Random matrices in physics. *SIAM review* **9**(1), 1–23 (1967)
- [46] Cerruti, N.R., Tomsovic, S.: A uniform approximation for the fidelity in chaotic systems. *Journal of Physics A: Mathematical and General* **36**(12), 3451 (2003)
- [47] Guhr, T.: Transition from poisson regularity to chaos in a time-reversal noninvariant system. *Physical review letters* **76**(13), 2258 (1996)
- [48] Michler, M., Bäcker, A., Ketzmerick, R., Stöckmann, H.-J., Tomsovic, S.: Universal quantum localizing transition of a partial barrier in a chaotic sea. *Physical*

Review Letters **109**(23), 234101 (2012)

- [49] Berry, M.V., Robnik, M.: Semiclassical level spacings when regular and chaotic orbits coexist. *Journal of Physics A: Mathematical and General* **17**(12), 2413 (1984)
- [50] Srivastava, S.C., Tomsovic, S., Lakshminarayan, A., Ketzmerick, R., Bäcker, A.: Universal scaling of spectral fluctuation transitions for interacting chaotic systems. *Physical review letters* **116**(5), 054101 (2016)
- [51] Pandey, A., Mehta, M.: Gaussian ensembles of random hermitian matrices intermediate between orthogonal and unitary ones. *Communications in Mathematical Physics* **87**(4), 449–468 (1983)
- [52] Bohigas, O., Giannoni, M.-J., Almeida, A.O., Schmit, C.: Chaotic dynamics and the goe-gue transition. *Nonlinearity* **8**(2), 203 (1995)
- [53] Fyodorov, Y.V., Mirlin, A.D.: Statistical properties of eigenfunctions of random quasi 1d one-particle hamiltonians. *International Journal of Modern Physics B* **8**(27), 3795–3842 (1994)
- [54] Bohigas, O., Giannoni, M.: Level density fluctuations and random matrix theory. *Annals of Physics* **89**(2), 393–422 (1975)